International Journal of Fatigue 199 (2025) 109060

Contents lists available at ScienceDirect

International Journal of Fatigue

journal homepage: www.elsevier.com/locate/ijfatigue

Enhanced local fatigue approach for welded tubular joints using 3D digital scans and implicit gradient model

Tim Brömer [a,*], Viktor Widerspan [b], Sulaiman Shojai [a,c], Elyas Ghafoori [a,b]

[a] Leibniz University Hannover, Institute for Steel Construction, ForWind, Hannover, Germany
[b] Fraunhofer Institute for Wind Energy Systems, Hannover, Germany
[c] German Aerospace Center (DLR), Institute of Maritime Energy Systems, Geesthacht, Germany

ARTICLE INFO

Keywords:
3D digital images
Welded tubular joint
High-cycle fatigue assessment
Notch stress approach
Residual stresses
Offshore wind turbines
Lifetime extension
Digitalization
Sustainability

ABSTRACT

The design of jacket structures in offshore wind turbines (OWTs) is driven by fatigue, crucial due to dynamic loads from operational movements, waves, and wind. This study aims to develop a digital framework for fatigue analysis of tubular welded joints in jacket OWT, incorporating real 3D scanned geometries and imperfections through their digital images. Numerical analysis has been conducted using finite element method to predict the experimental results, in which the effect of micro-support has been taken into account using an implicit gradient model (IGM). Furthermore, 4R method has been used to account for mean stress corrections due to residual stresses and imperfections. Digital Image Correlation (DIC) was employed during the high-cycle fatigue experiments to detect the initiation and progression of a technical crack, providing precise measurements of strain distribution and crack size development. The results have shown that the proposed numerical framework based on the IGM can successfully determine the lifetime and location of crack initiation in the 3D scanned welded details. The proposed framework significantly improves the accuracy of high-cycle fatigue life predictions and offers a scalable solution for structural health monitoring, facilitating lifetime extension across a wide range of industries, including construction, automotive, aerospace, and renewable energy.

1. Introduction

Welding is a cornerstone in engineering, enabling the assembly of various structural components across multiple disciplines, including civil, mechanical, aerospace and offshore engineering. In applications ranging from bridges, cranes and skyscrapers to pressure vessels and ships, welding ensures structural integrity and durability. In offshore engineering, welded connections are particularly critical due to the demanding environmental conditions and high cyclic loads. This is especially true for Offshore Wind Turbines (OWTs), where support structures like jacket foundations play a vital role. Jacket foundation structures are constructed as lattice frameworks with three or four legs made from hollow sections. They offer the benefit of high rigidity while utilizing relatively low amounts of material [1,2]. These properties play a major role in the offshore sector and result in a transition from monopiles to jacket foundations as offshore wind farms are located further away from shore and in greater water depth up to 60 m [3]. During their service life, support structures for OWTs are exposed to high cyclic loads due to mainly movement of the turbine during operation, waves and wind. Therefore, the fatigue strength of the structure is the design driving factor, especially for the components of the jacket, which exhibit high stress concentrations, such as the welded tubular joints between the chord and the brace. One idea is therefore to reduce the notch sharpness of the weld seams with a new design-weld, in order to reduce the stress concentrations. The same idea has already been pursued with casted tubular joints and is anchored with its own S-N curves in the DNV-RP-C203 guideline [4]. However, this approach has not been able to fully establish itself due to high internal imperfections of the casted joints.

The DNV-RP-C203 guideline [4] provides the most crucial normative regulation for the practical fatigue verification of offshore jacket tubular joints. This guideline utilizes the structural stress approach (SSA), a well-established method in the oil and gas industry for decades, and combines it with the relevant structural stress S-N curve T found in [4]. To determine the S-N curves, a large number of fatigue tests have been carried out in the past to quantify the fatigue strength of tubular joints. The results of these tests can be found in the OTH 92 390 report [5].

* Corresponding author.
E-mail addresses: broemer@stahl.uni-hannover.de (T. Brömer), viktor.widerspan@iwes.fraunhofer.de (V. Widerspan), sulaiman.shojai@dlr.de (S. Shojai), ghafoori@stahl.uni-hannover.de (E. Ghafoori).

https://doi.org/10.1016/j.ijfatigue.2025.109060
Received 27 January 2025; Received in revised form 14 April 2025; Accepted 12 May 2025
Available online 12 May 2025

Nomenclature

OWT	Offshore Wind Turbine
SSA	Structural Stress Approach
NSA	Notch Stress Approach
IGM	Implicit Gradient Model
FEM	Finite Element Method
DIC	Digital Image Correlation
ENS	Effective Notch Stress
SWT	Smith, Watson and Topper
R-O	Ramberg-Osgood
UML	Uniform Material Law
WPS	Welding Procedure Specification
NURBS	Non-Uniform Rational B-Splines
TCD	Theory of Critical Distance
STL	Stereolithography
σ_k	Elastic notch stress
σ_f	Effective notch stress
ρ^*	Microstructural support length
ΔK_{th}	Fatigue propagation threshold
$\Delta\sigma_0$	Fatigue limit
ρ_{ref}	Reference radius
G	Weighting function
Ψ	Scaling factor
∇^2	Laplacian operator
R_{local}	Local stress ratio
$\Delta\sigma_f$	Effective notch stress range
$\Delta\sigma_{f,ref}$	Mean stress corrected effective notch stress
H	Strength coefficient
n	Hardening coefficient
H'	Cyclic strength coefficient
n'	Cyclic hardening coefficient
R_m	Tensile strength
$R_{p0.2}$	Yield strength
F_o	Upper force limit
F_u	Lower force limit
N	Number of load cycles
Δy	Distance between sections along y-axis
σ_N	Nominal stress
$\dot{p}$	Heat flux
a	Weighting parameter (IGM)
Λ	Conductivity parameter
C_p	Specific heat capacity
ρ_d	Specific heat density
ρ_f	Fictitious notch radius
K_f	Effective notch factor
$K_{f,initial,max}$	Maximum notch factor at location of maximum elastic notch factor
$K_{f,crack}$	Effective notch factor at crack location
$K_{f,Neuber}$	Effective notch factor from Neuber model
$K_{f,IGM}$	Effective notch factor from IGM
r_{brace}	Radius of brace
t_{brace}	Thickness of brace
E	Young's modulus
C_f	Fatigue capacity (4R)
m	Slope of SN-curve
$N_{f,cal}$	Calculated load cycles until crack initiation
$N_{f,exp}$	Load cycles until crack initiation from experiments

Here, the failure criterion "through-thickness crack" was applied and structural stresses were determined using linear extrapolation. Further tests by Van Wingerde et al. [6] support the findings and the S-N curves from [5]. The tubular joints in these investigations were always manually welded, while Zilli et al. [7] and Schürmann [8] also applied SSA on automated welded joints. However, a huge drawback of the SSA is the fact that all properties related to the "as-built" weld geometry cannot be taken into account.

This can be overcome with consideration of the local weld geometry within the notch stress approach (NSA). This procedure is included in DNV-RP-C203 [4], IIW [12] and DIN EN 1993–1-9 [13] and is summarized in Radaj et al. [14]. The application of the NSA based on the guidelines mentioned is not possible without further ado, as a crack can occur not only in the area of the weld toe but also between individual weld layers. In addition, the NSA cannot be applied to large-scale nodes with a through-thickness crack as a crack criterion. In this case, a further approach would be a type of two-phase model that combines the NSA with a fracture mechanics approach. This would allow the service life of a structure up to the technical crack initiation to be determined using the NSA and the crack propagation to be calculated further using linear fracture mechanics – ideas in this direction already exist using local approaches [15]. Additionally, to the weld seam geometry, factors such as the micro-support effect in the form of an effective notch factor or residual stresses and material characteristics can also be taken into account within application of local fatigue approaches, as seen in [16–18].

This work presents a framework for determining the fatigue strength of welded tubular joints based on the weld geometry. For this purpose, it focuses on the NSA, how to consider residual stresses according to the method of Nykänen and Björk [19] and to apply this method to manually welded tubular joints, which were tested under cyclic loading. Notch stresses are determined using 3D scans that thoroughly consider both the overall structural misalignments of the joint and the detailed weld geometry. The use of modern 3D scanning technology provides highly detailed geometric data, capturing surface irregularities and real-world imperfections that significantly influence fatigue behavior, which conventional methods often overlook. This ensures a more accurate representation of structural components, enabling precise fatigue life predictions and reducing uncertainties in the assessment process. The use of 3D scans for fatigue assessment is widespread and has already been carried out by Larsen [20] and Plets [21], for example. The problem with this approach, however, lies in correlating the results with the fatigue strength of the components in a meaningful way. One approach from Schürmann [8] is to consider the micro-support effect via the IGM, which is why the fatigue effective notch stresses are derived according to this model introduced by Peerlings [22] and carried out according to Lang [23]. In addition, Schürmann [8] leaves out the detailed influence of residual stresses and mean stress, which are further examined via 4R method in this paper. The highlights of this study can thus be summarized as follows:

- Creation of digital modelling framework of welded tubular joints in order to take into account the real weld seam geometries and misalignments of the entire node, precise 3D digital scans capture detailed geometry and real-world imperfections, enabling more accurate fatigue predictions and reducing uncertainties compared to conventional techniques
- Consideration of effective notch stresses via IGM on the basis of digital models for welded tubular joints
- Validation of IGM by comparison of the locations with maximum elastic notch stress and of crack initiation observed by DIC during high-cycle fatigue tests

- Use of the NSA including residual stresses for welded tubular joints for fatigue assessment and determination of the service life up to a defined technical crack criterion

2. Theoretical background

Weld seams are the critical details of connections made from circular hollow sections (CHS) that determine the design of the entire structure. On the one hand this is due to changes in material properties and residual stresses resulting from the welding process and on the other hand to stress concentrations caused by geometric notches in the weld seam itself. The aim of the local fatigue approach used here is to consider the stress concentrations based on the geometry, the residual stresses from the welding process and local material behavior at the notch base. The approach is based on the widely used notch stress method developed by Neuber and Radaj [14,24]. For this purpose, effective notch stresses are calculated according to the notch stress method, taking into account the micro-support effect, and these are integrated in the so-called 4R method according to Nykänen and Björk [19,25]. The next sections provide detailed description of each of the proposed methods.

2.1. Notch stress analysis methods

In the NSA, elastic notch stresses σ_k at the failure-critical location are calculated on the basis of the theory of elasticity. Unlike the SSA, which is widely used for CHS nodes, this approach is based on the local stress at the weld toe or the weld root assuming micro-support effects. These micro-support effects describe the fact that it is not the maximum elastic notch stress that is decisive for crack initiation or crack propagation, but a lower non-local stress. The basis for this realization is the fact that the yield point of the material can be exceeded, particularly at sharp notches, and microcracks can be initiated without further crack propagation occurring – the local yielding therefore reduces the stress concentrations [14,26]. For this reason, the concept is often referred to as the effective notch stress (ENS) concept.

The open literature presents a variety of different methods for calculating the effective notch stress σ_f, which can be used to take the micro-support effect into account. One of the first methods is the approach according to Neuber [27], which describes the effective stress as a function of the microstructural support length ρ^*. The stress σ_f can thus be calculated as the mean value of the elastic stress field

$$\sigma_f = \frac{1}{\rho^*}\int_0^{\rho^*} \sigma(x)dx \tag{1}$$

This method can also be referred to as the line method according to Taylor's Theory of Critical Distance (TCD) [28]. In order to avoid the process of integrating the stress field, Neuber proposes in [27] the use of a reference radius instead of the real radius. In this way, the effective stress from Eq. (1) equals the maximum calculated stress taking into account the reference radius. This radius results in

$$\rho_f = \rho_{real} + s\rho^* \tag{2}$$

and differs depending on the load case and strength hypothesis, which is taken into account using the parameter s. Fig. 1 shows the relationship between the notch radius and the reference radius presented in more detail. The microstructural support length ρ^* depends on the material and its microstructural condition and can be expressed by the fatigue crack propagation threshold ΔK_{th} and the fatigue limit $\Delta\sigma_0$ [29].

$$\rho^* = \frac{2}{\pi}\left(\frac{\Delta K_{th}}{\Delta\sigma_0}\right)^2 \tag{3}$$

To extend the reference radius approach proposed by Neuber [27] to welded joints, the parameter s is assumed to be 2.5 for plain strain conditions and combined with the von Mises multiaxial strength criterion by Radaj [30]. Considering welds in mild steel, the value $\rho^* = 0.4$ mm is appropriate. This assumption stems from a worst-case assessment assuming a real notch radius of zero, so that the reference radius is now $\rho_{ref} = 1$ mm. This procedure has been proven to be applicable to welded joints and is a standardized procedure within the IIW design recommendations [12].

2.2. Implicit gradient model

The IGM is another approach to calculate effective notch stresses – the already described stress averaging via the microstructural support length ρ^* (Eq. (1)) is analogous to this, which according to Bažant [31] and further by Zhang [32] is described using a weight function G and a scaling factor Ψ:

$$\sigma_f(x) = \frac{1}{\Psi(x)}\int_V G(x,y)\sigma_k(y)dV_y \tag{4}$$

Furthermore, V is the volume around the notch, x the point of interest and y the far point. By averaging the calculated notch stress over a certain volume using a Gaussian weighting, the IGM is introduced [22]. The integral relation Eq. (4) is transformed into a differential approximation by substituting a truncated Taylor expansion for the local stress in Eq. (4). The resulting model is a Helmholtz equation and can be described as:

$$\sigma_f(x) = a\nabla^2\sigma_f(x) = \sigma_K(x) \tag{5}$$

where $a > 0$ and ∇^2 denotes the Laplacian operator. The detailed derivation of this equation can be found in [22]. To solve Eq. (5)

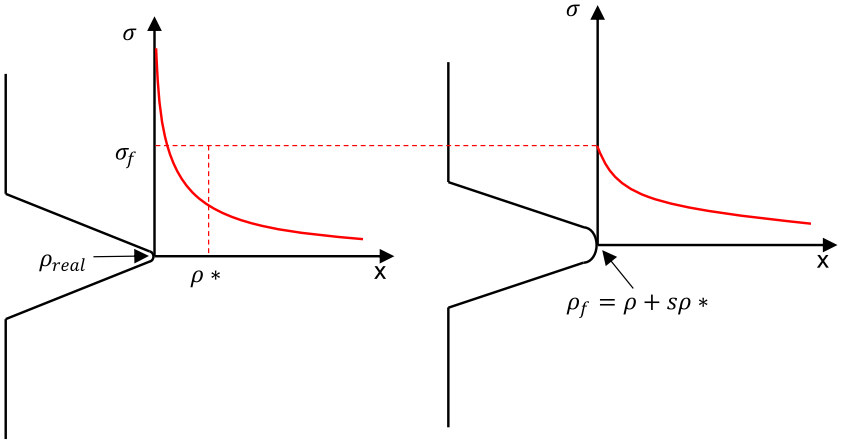

Fig. 1. Illustration of the concept of reference notch radius.

numerically, an appropriate boundary condition must be considered. Here, the volume of the body is considered as domain and the surface has to be defined as boundary, usually done by the Neumann boundary condition:

$$\frac{\partial \sigma_f(x)}{\partial x} \cdot n = 0 \tag{6}$$

According to Lang [23], Eq. (5) can be interpreted as a transient heat conduction equation in order to use a commercial finite element solver to solve it for a discrete timestep $\Delta t = 1$ s. With this procedure, the linear elastic notch stress is used as the initial temperature in a transient thermal conduction calculation to calculate the fatigue effective notch stresses. With the help of the IGM, it is therefore possible to calculate fatigue effective stresses for each location of the real scanned geometry and the user is not dependent on a single local value or the creation of a model, as is the case with the SSA or the reference radius approach proposed by Neuber, for example.

2.3. 4R method for residual and mean stresses

The so-called 4R method according to Nykänen and Björk [19,25] is used to take into account various influences on the fatigue strength of components, in particular welded joints made of steel, in the fatigue strength assessment process. Particularly relevant here is the consideration of residual stresses and mean stress correction, which can affect the fatigue resistance. In the IIW design recommendations [12], this is considered by multiplying the fatigue class of classified details by a fatigue enhancement factor $f(R)$.

Another approach is the mean stress correction according to Smith, Watson and Topper (SWT) [33], which supports the hypothesis that there is a stress–strain function governing the fatigue of metals. This function is dependent on the product $\sigma_{max}\varepsilon_a$, where σ_{max} is the maximum tensile stress and ε_a is the strain amplitude. Nykänen and Björk [19,25] implemented the SWT correction in a novel way by transforming the linear elastic notch stress to local cyclic elastic–plastic material behavior from which the local stress ratio R_{local} can be obtained and a mean stress-corrected reference notch stress range is formulated as

$$\Delta\sigma_{f,ref} = \frac{\Delta\sigma_f}{\sqrt{1 - R_{local}}} \tag{7}$$

The local stress ratio R_{local} can be expressed as

$$R_{local} = \frac{\sigma_{min}}{\sigma_{max}} \tag{8}$$

The point of maximum stress σ_{max} is determined using the initial load step via the Ramberg-Osgood (R-O) curve [34] by converting the determined elastic stresses into elastic–plastic values via the Neuber hyperbola. In this step, the equation

$$\frac{\left(\sigma_k + \sigma_{k,res}\right)^2}{\sigma_{max} E} = \frac{\sigma_{max}}{E} + \left(\frac{\sigma_{max}}{H}\right)^{\frac{1}{n}} \tag{9}$$

is set up to calculate the strain ε and resolved according to the stress σ_{max}. The parameters H and n describe the strength coefficient and the hardening coefficient. When kinematic hardening is assumed, a cyclic material behaviour including the cyclic R-O curve and accordingly also the Neuber hyperbola (see Fig. 2) with cyclic parameters can be assumed:

$$\frac{\Delta\sigma_k^2}{\Delta\sigma E} = \frac{\Delta\sigma}{E} + 2\left(\frac{\Delta\sigma}{2H'}\right)^{\frac{1}{n'}} \tag{10}$$

Equation (10) is similar to Equation (9), the difference here lies in the consideration of the range values with Δ and H' and n' represent the cyclic strength coefficient and the strain hardening exponent, whereby the coefficients $H' = H$ and $n' = n$ can be assumed for a fatigue life with more than 50,000 cycles [15].

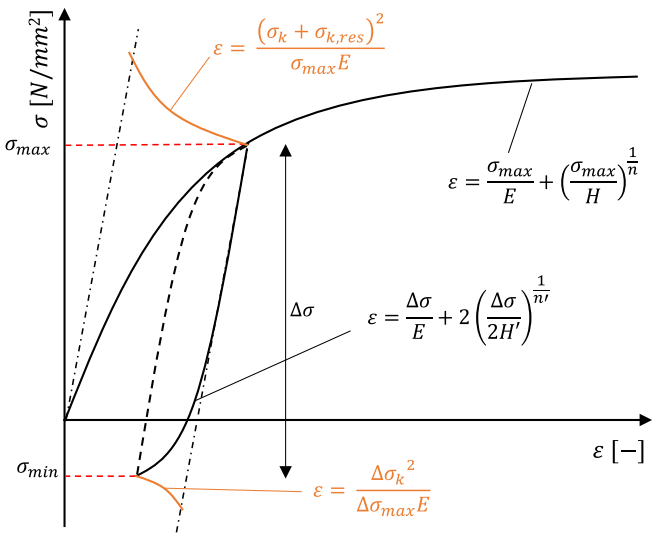

Fig. 2. Procedure of calculating the local mean stress ratio R_{local} according to the 4R method including Neuber hyperbole (orange) and R-O-curve (black). (For interpretation of the references to colour in this figure legend, the reader is referred to the web version of this article.)

The cyclic strength coefficient and the strain hardening exponent are based on various assumptions in the literature, see Table 1. for different examples. The so-called Uniform Material Law (UML), which was calibrated on the basis of tests according to Bäumel and Seeger [9], is widely used. Based on this, the UML was modified as part of the German guideline "Richtlinie Nichtlinear" [10]. In addition, parameters relating to correlations and relationships among hardness, tensile properties and cyclic deformation properties were determined in [11].

The entire procedure of the 4R method for calculating the mean stress corrected reference notch stress range, taking residual stresses into account, is shown in Fig. 2.

3. Experiments

3.1. Jacket node fabrication

As part of a German national research project (acronym "SmartWeld"), fatigue tests were conducted on scaled jacket nodes at the Test Centre Support Structures Hannover. The tubular joints are made from welded circular hollow section tubes in S355 G10 + M steel, which is a typical material used in offshore structures. The scale of the joints is approximately 1:2 in comparison to real structures, and all other dimensions and properties can be found in Fig. 7. The braces are manually welded to the chords using the MAG process according to DIN EN ISO 4063. The edges are prepared for welding by clean blasting, brushing, and grinding. The electrodes T46 2P C1 H5/T46; Ti 52 T-FD and protective gas M21 ArC 18 (82% Ar/18% CO2) were used for welding [35]. All the tubular joints were welded with a Welding Procedure

Table 1
Values of the cyclic strength coefficient and the strain hardening exponent according to different publications [9,10,11].

	$H'[MPa]$	$n'[-]$
UML [9]	$1.5R_m = 753$	0.15
Modified UML [10]	$\frac{3.1148MPa\left(\frac{R_m}{MPa}\right)^{0.897}}{0.338^{0.187}} = 1009.38$	0.187
Lopez and Fatemi [11]	$3{*}10^{(-4)}R_m^2 + 0.23{*}R_m + 619 = 810.06$	$-0.33\frac{R_{p0.2}}{R_m} + 0.4 = 0.117$

Specification (WPS) and a welding quality conforming to DIN EN 1090–2 [36] with a welding configuration comprising two-thirds single bevel butt weld and one-third fillet weld and welded on only one side.

3.2. Fatigue tests

The tubular joints were subjected to fatigue loading with a sinusoidal load and frequency of 1.5 Hz in the tensile range ($R = 0.1$) until through-thickness crack was detected, which serves as the failure criterion. This crack was detected by monitoring the inner air pressure in sealed chord. The pressure was reduced by ca. 0.5 bar with a vacuum pump. A rapid change in pressure indicates that the joint has ruptured. This detection method allows for identifying both externally visible through-thickness cracks in the chord as well as cracks in the chord's wall thickness initiating at the weld root. The test setup is shown in Fig. 3 and further information regarding the boundary conditions of the fatigue test can be found in Fig. 9 This methodology was also used in another German national research project (acronym "FATInWeld") [8].

Prior to conducting the tests, the most highly stressed area – identified as the location with the greatest stress concentration within the structure of the tubular joint – was determined using a FE model that includes the geometry of the welded tubular joint and a rough weld geometry. Stochastic black-white speckle pattern was applied to this hotspot-area, in order to monitor strains with digital image correlation (DIC). The DIC system is mounted on a separate truss structure in order to be independent of all movements during the testing procedure. It provides detailed information on the strain state directly at the notch of the weld seam and enables to monitor the crack initiation and propagation. It should also be noted that the test specimens were not exposed to environmental influences from the surroundings over a longer period of time. Therefore, a potential influence of corrosion on the results of the fatigue tests is excluded and not addressed further.

3.3. DIC measurements

Using the DIC system, strains were recorded during the fatigue tests, providing insights into the crack location, crack initiation, and the crack propagation phase. The notch stress method used in this study aims to evaluate the number of load cycles until joints fracture. It's important to note that this method, along with the S-N curves, was developed based on small-scale specimens tested by Seeger et al. [37,38] with an approximate width of 40 mm. The tubular joints analyzed here represent larger structures, and applying the notch stress concept with the failure criterion of through-thickness crack could yield overly conservative results [39]. Therefore, similar to the approach in [39,40], it is assumed that the fracture of a small-scale fatigue test specimen corresponds to crack initiation in a large-scale structure. Hence, in this study, technical crack is defined as the point in time at which a crack enters the progression phase and has a width of 40 mm. Fig. 4 illustrates the criterion of the technical crack and may help to better understand this assumption.

For further numerical analyses, it is necessary to determine the number of load cycles up to the development of the technical crack. Various criteria can be used for the evaluation, for example local strain peaks or sudden changes in displacement along a path perpendicular to the weld seam [41]. Additionally, several studies have adopted locally measured strains of 1% or greater as the criterion for technical crack formation [42,43]. In this study, formation of a crack is localized using the displacement along the defined path. Once a crack is localized, adjacent sections are examined to determine its actual length. The evaluation procedure is schematically illustrated in Fig. 5. In each step of the DIC analysis, sections are analyzed at approximately 1 mm intervals to assess the location of crack initiation and the length of the resulting crack..

3.4. Test results

3.4.1. Fatigue test results

A total of three different jacket nodes were tested, but only two nodes, referred to as B1 and B2, are suitable for further evaluation. Node B3 cannot be analyzed due to the formation of cracks at its lower weld seam with no DIC. Consequently, no data from the strain gauges or the DIC system are available for crack initiation and propagation on B3. Only the stress range and the number of load cycles at fracture are known for this specimen. The results of the tests including upper (F_o) and lower (F_u) load as well as the number of load cycles up to through-

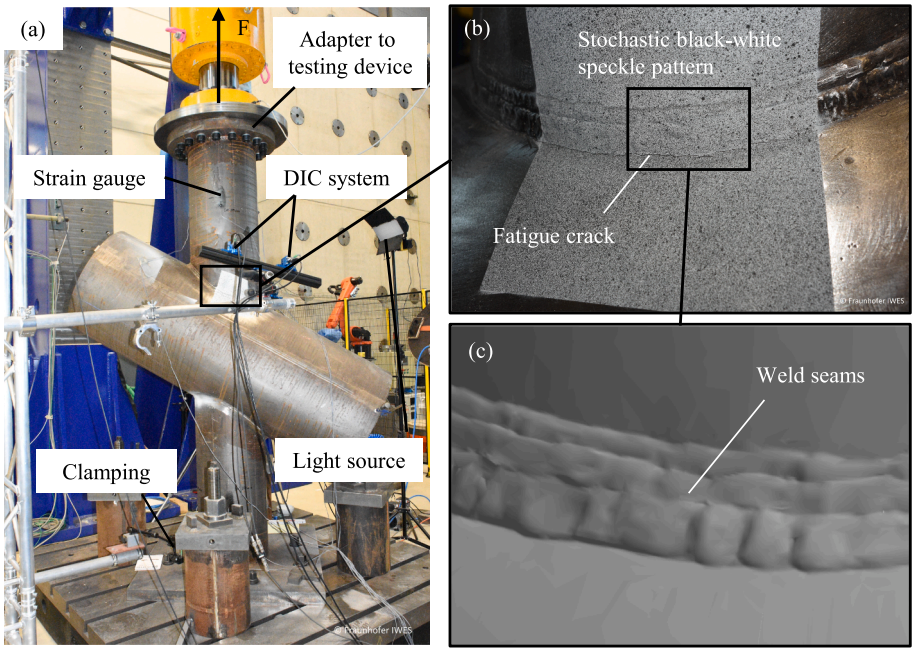

Fig. 3. (a) Test setup for the axial fatigue tests of the tubular X-joints with Limess DIC system, (b) stochastic black-white speckle pattern for DIC measurement and (c) weld seam geometry extracted from scans.

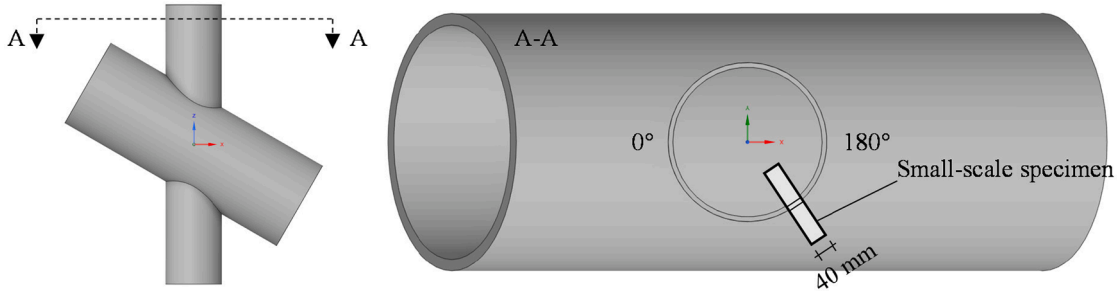

Fig. 4. Derivation of the technical crack criterion for the welded tubular joints based on the fatigue tests on 40 mm small scale specimens tested by Seeger et al. [37,38].

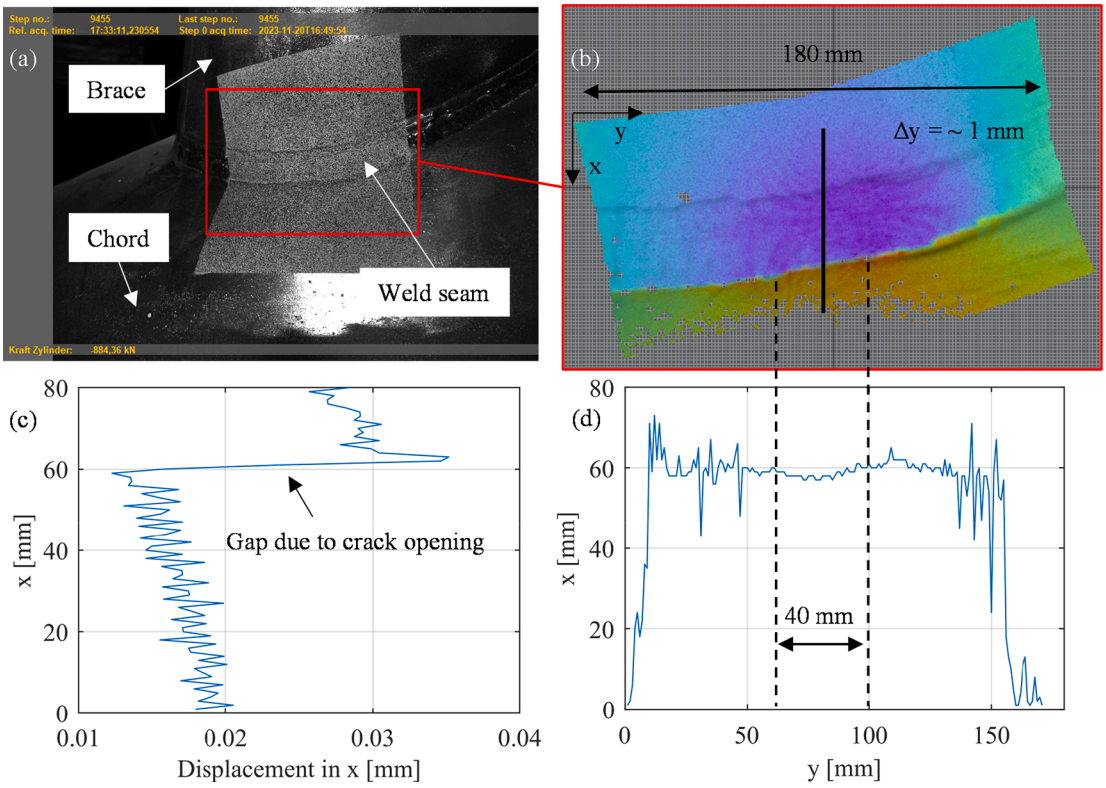

Fig. 5. (a) Stochastic black-white speckle pattern at fatigue relevant location, (b) investigation of displacement using equidistantly arranged sections with a distance of approximately 1 mm, (c) displacements in x along x-coordinate of one section and (d) crack length detection of 40 mm – all exemplary for sample B1.

thickness crack are summarized in Table 2. During the tests, an R-ratio of 0.1 was targeted, but this target could not be precisely achieved due to internal control parameters of the hydraulic system of the 2 MN actuator (Fig. 3(a)) affecting the underload values.

The results of the fatigue tests can then be analyzed using S-N curves. According to current offshore standards, welded tubular joints are dimensioned for through thickness cracking utilizing the SSA. The evaluation is therefore carried out using the structural stresses. The required structural stress ranges $\Delta\sigma_S$ are based on the SCF values determined numerically as an extrapolation of the stresses normal to the fatigue-critical weld notch according to DNV-RP-C203 [4].

Table 2
Results of fatigue tests for specimens B1, B2 and B3.

Specimen	$F_o[kN]$	$F_u[kN]$	N [-]
B1	900	90	310,500
B2	870	70	490,000
B3	700	40	478,000

$$SCF = 3.15 \tag{11}$$

The SCF value for the crown position shows a significantly lower value with 1.4 – both values lie in good agreement with the SCFs according to the analytical formulas from DNV-RP-C203 [4], which result in 2.79 for the saddle and 1.64 for the crown positions. The statistical analysis of the fatigue tests follows the procedure outlined in the background documentation 9.01 of DIN EN 1993–1-9 [13] fatigue design rules, as referenced by the ECCS Technical Committee 6 [44]. Generally, it is assumed that the results follow a student's t-distribution and the evaluation is carried out for a survival probability of 97.7%. However, as only three test results are available in this study, the application of the student's t-distribution leads to a scattering, which would result to an unrealistic low fatigue strength for a survival probability of 97.7%. Therefore, the 50% survival probability is used for representing the test results. In addition, the T S-N curve from DNV-RP-C203 [4], which represents the currently valid S-N curve for welded tubular joints, is used for comparison, see Fig. 6.

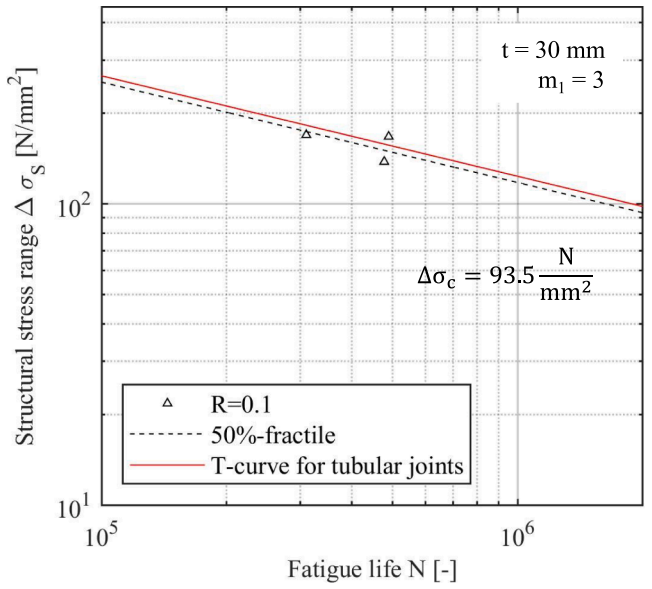

Fig. 6. Fatigue test result evaluation for the manually welded tubular X-joints considering through thickness cracking.

The statistical analysis of the three test specimens shows that the 50%-fractile is slightly below the T S-N curve. The size effect according to current offshore standards was taken into account, which reduces the initial T curve by a ratio of the actual thickness $t = 30$ mm to the reference thickness $t = 16$ mm. In addition, a constant gradient was assumed in the statistical evaluation of $m = 3$. This results in a mean fatigue strength of the welded joints of $\Delta\sigma_C = 93.5$ N/mm^2 compared to the value of the reduced T S-N curve with 98.4 N/mm^2. In the course of the project, further welded tubular joints will be tested, which will be evaluated via the S-N curve and increase the statistical bandwidth.

3.4.2. DIC measurement

The procedure described in the previous section for determining the number of load cycles up to the development of a technical crack provides the results shown in Table 3. It is noticeable that the crack initiation phase is relatively short when comparing the number of load cycles up to crack initiation versus up to through-thickness crack in the joints. The technical crack occurs after approximately 17% of the experienced load cycles up to the through thickness crack. It can therefore be assumed that microcracks are already present in the area of the weld seam notch before the start of the fatigue test and continue to propagate with the experienced load cycles.

Schürmann [8] also investigated different stages during the fatigue test of tubular joints and identified the crack initiation phase as approximately 20% of the total service life of the structure based on a 1 mm crack definition. For the joints examined here, the phase duration is in a similar range, although the crack criterion was a crack length of 40 mm (Fig. 5), instead of a 1 mm crack. Consequently, the crack initiation phase is even shorter compared to Schürmann's smaller test specimens [8]. It should also be noted that with larger node dimensions, the desired working distance increases, leading to a decrease in the image resolution. As the quality of the speckle pattern including the speckles' size depends on the camera resolution and is essential to the accuracy of the measured displacements, all parameters must be synchronized.

Table 3
Results of the presented routine for determining the number of load cycles up to a technical crack of 4 cm for specimens B1 and B2.

Specimen	$N_{Crack,4cm}$ [−]	$N_{Failure}$ [−]	$\frac{N_{Crack,4cm}}{N_{Failure}} \cdot 100$ [%]
B1	54,000	310,500	17.39
B2	85,000	490,000	17.35

4. Numerical analysis and micro-support effect

4.1. Development of numerical model from 3D digital scans

The development of the numerical model for tubular joints consists of several steps to ensure high accuracy and detail. First, a digital model is generated by scanning the joints from various angles using a GOM ATOS Q 3D scanner. This process captures detailed scans of the weld seam and overall imperfections of the node. The data is compiled into an STL file. During scanning, the working distance is set at 49 centimeters, and the distance between data points ranges from 0.03 to 0.12 mm. The STL file includes a triangulated mesh between these points as a model of the joints outer surface. To maintain precision, the digital model contains higher resolution scans specifically for the fatigue-critical area of the weld seam notch, the smallest distance between the data points is selected and a scanning residency of 0.005–0.01 mm can be achieved.

In the next step, the STL model must be converted into a solid model to carry out a numerical analysis. This is accomplished through a reverse engineering process, which creates a continuous surface in the model, thereby avoiding singularities during the numerical analysis. This process also reduces the large number of data points, lines, and facets present in the STL model, while maintaining the detailed scans of the weld seam.

The reverse engineering process begins with determining the patch size and the fineness of the grid for the non-uniform rational B-splines (NURBs) in both the x and y directions. Based on previous investigations, a patch size of 20 × 20 mm with a grid of 90 curves is suitable, as no significant changes in stresses are expected beyond this configuration [17]. Using these parameters, the detail scans of the weld seam – which particularly critical for fatigue analysis – can be approximated with NURBs. As the inner surface of the welded tubular joints could not be recorded during the scan, the inner surface was reconstructed by using the thicknesses and inner radii of the tubes. To achieve this, all outer surfaces were shifted inwards by the nominal thickness of the tubes. This ensured that the thickness of the tube is achieved and coarse misalignments, such as axial misalignment, offset and deviation from the perfectly round tube, can be taken into account in the reverse engineering process.

For illustration, Fig. 8 shows the deviations of the CAD model from the scanned model. To do this, the CAD model and the scan of the real welded joint were superimposed in the GOM Correlate software and approximated using a best-fit procedure. The result shows that the largest deviations between the surface of the scan and the CAD model for node B1 and node B2 are in the area of the weld seams between the brace and chord and the weld seams of the tubes. This is obvious, as the design-welds are not taken into account in the CAD model.

This approach ensures that all relevant details of the geometry, as well as imperfections of the entire structure, are accurately captured in the digital model. Subsequently, the solid model can be meshed, provided with boundary conditions, and used for numerical analysis, as illustrated in Fig. 9 (a) and (b).

For the numerical calculations, an axial force is applied to the upper brace, and its magnitude is equal to the value of the tube's cross-sectional area in mm^2. This setup ensures that the nominal stress in the brace reaches the value $\sigma_N = F/A = 1$ MPa. As a result, stress concentrations can be directly observed from the calculation.

Furthermore, the lower brace is firmly clamped to prevent displacements in the x, y and z directions, reflecting the conditions of the test setup. Tetrahedron-shaped elements with quadratic shape functions are used to mesh the geometry, allowing for a sufficiently detailed representation of the weld seam. This type of element is particularly suitable for meshing of complicated models based on real geometries in order to capture the notches and radii relevant for fatigue. Initially, a

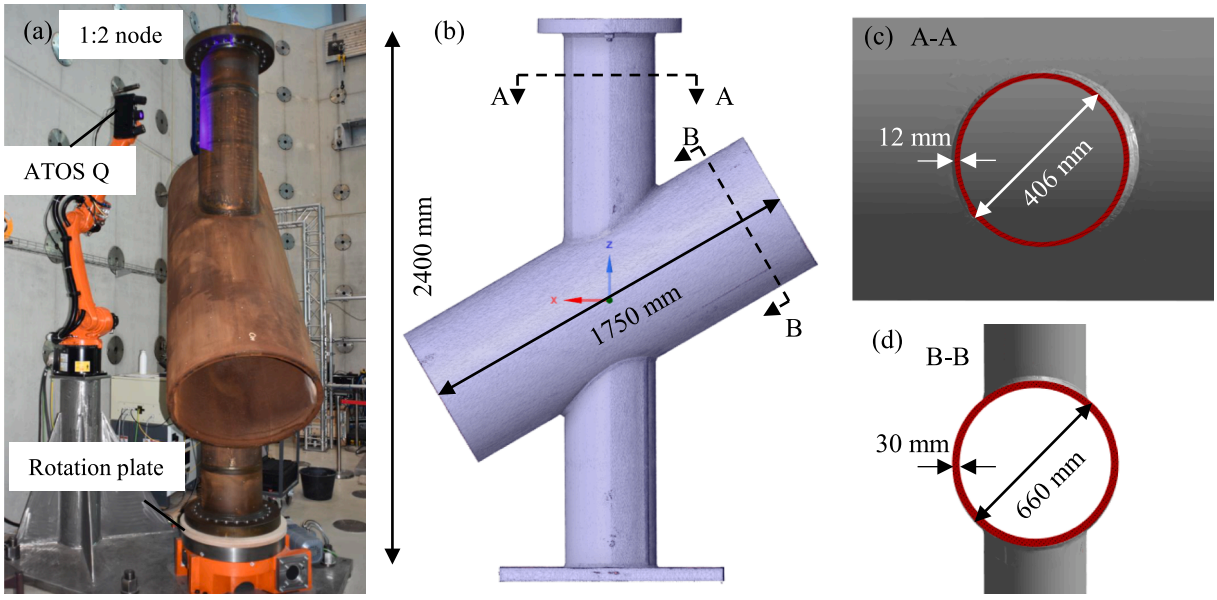

Fig. 7. Scanning process shown for a CHS joint, (a) ATOS Q 3D scanner mounted on a robot, (b) STL file resulting from multiple scans from different angles, (c) Section A-A with dimensions of the brace, (d) Section B-B with dimensions of the chord.

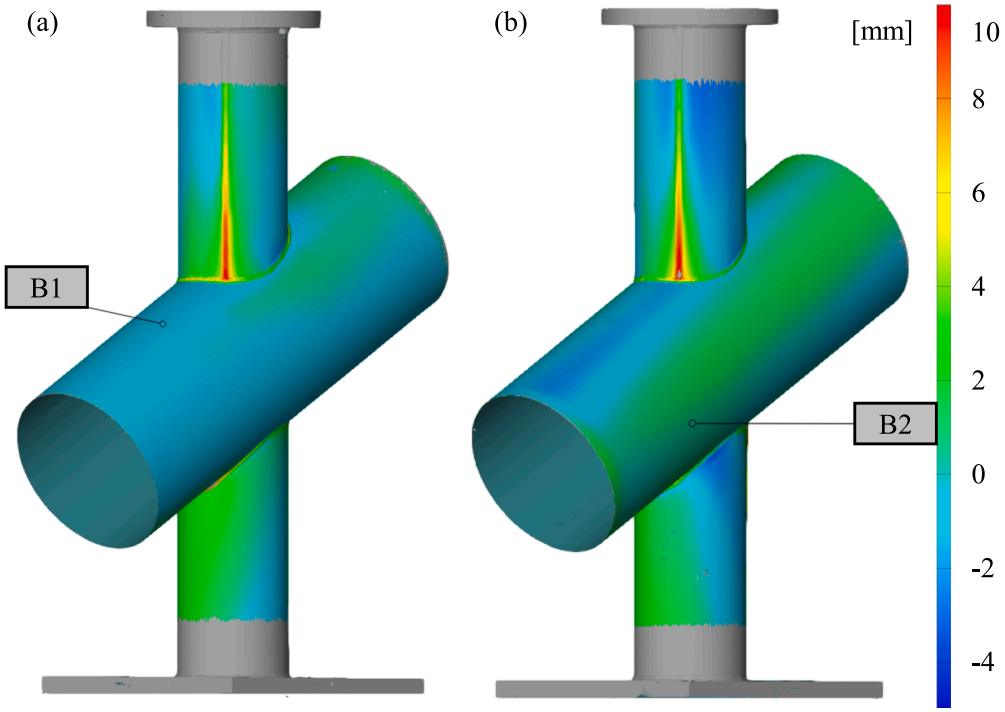

Fig. 8. Surface comparison between the CAD file of the welded tubular joint and the stl file of the 3D scan for (a) joint B1 and (b) joint B2.

coarse mesh is applied to the entire node model to determine global displacements, which are then transferred to a more detailed sub-model of the weld seam, as shown in Fig. 9 (b). To capture the stresses at the weld seam notch accurately, the element size is particularly small with an edge length of 0.15 mm. This element size is based on Lang's [23] recommendation to use a maximum length $< 2\sqrt{a}$ for square elements. As a specific value for the weighting parameter a from IGM is not specified at this stage, literature values for steel with $a \approx 0,01$ mm^2 are used [45].

4.2. Application of implicit gradient model

To account for the micro-support effect using the IGM approach, the differential equation (5) from section 2.2 must be solved. Based on the work of Lang et al. [46] and Lener et al. [47], this can be accomplished using the thermal analysis module within commercial FE-software, as equation (5) closely resembles the differential equation for thermal diffusion. In this research, the thermal analysis module in ANSYS Workbench is employed to solve equation (5). Elastic notch stresses are used as input values for the diffusion analysis at each node within the numerical model. The Neumann boundary condition, according to

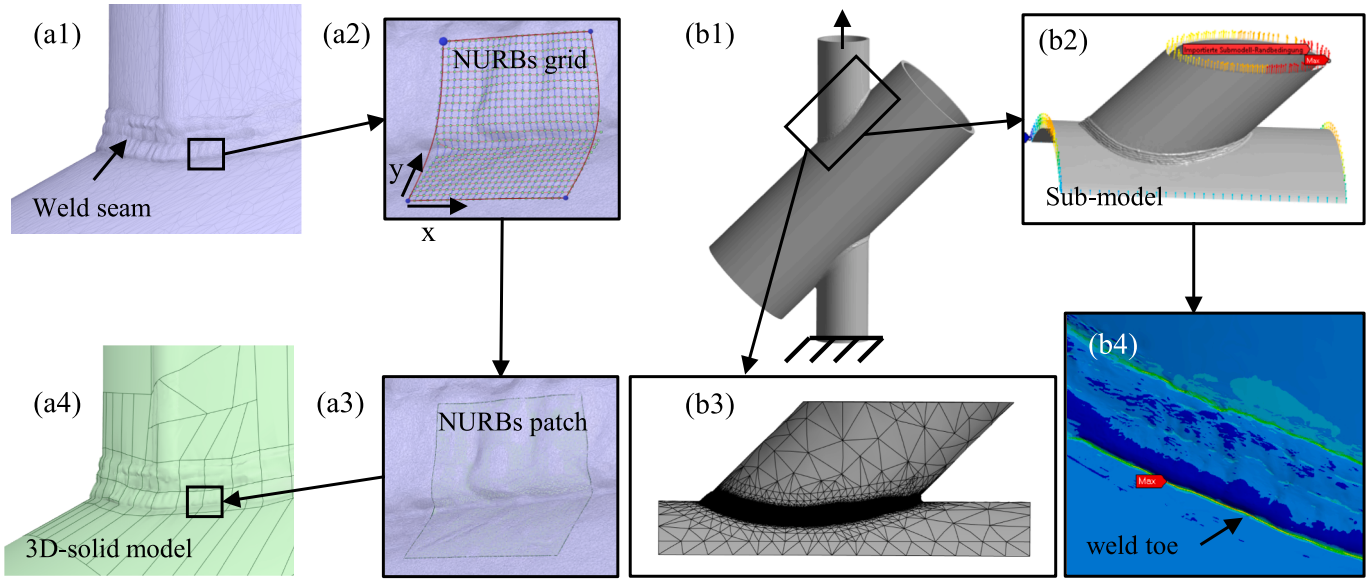

Fig. 9. (a) Process of using NURBs in ANSYS Spaceclaim to approximate the stl file with a continuous surface, (b1) boundary conditions for an axially loaded tubular joint, (b2) sub-model of the fatigue-critical area, (b3) meshed sub-model with 0.15 mm elements and (b4) results of an elastic calculation of the first principal stresses.

equations (6), is applied using a 'heat flux' boundary condition with $\dot{q} \approx 0$ to the specimen's surface. The weighting parameter a is associated with the thermal properties as $a = \frac{\lambda}{(\rho_d \bullet c_p)}$ and is assigned with the thermal conductivity parameter λ, while both the specific heat capacity and density are assigned values of $c_p = 1.0$ and $\rho_d = 1.0$, respectively.

4.2.1. Parameter study for a

Overall, there are different ways to determine the parameter a. Firstly, the parameter can be calibrated based on the assumptions of the TCD or the reference radius approach proposed by Radaj [30]. Previous studies [48,49] have demonstrated a correlation between intrinsic material length and the critical distance. The procedure for this approach, as outlined in [8,23], involves calibrating the parameter for a certain numerical model. This calibration is done by comparing the fatigue effective stress calculated using the notch rounding approach proposed by Radaj, which considers a fictitious notch radius of $\rho_f = 1$ mm, with the corresponding IGM-based fatigue-effective stress for an ideal sharp notch. The parameter a is then adjusted iteratively until a value is found that matches

$$K_{f,Neuber} = K_{f,IGM}(a) \tag{12}$$

Additionally, one can choose the weighting parameter a according to the literature and check its applicability by examining the locations of crack initiation. This procedure leverages the effect that as the value of parameter a increases, the calculated effective stress concentration changes. This is because the stresses are averaged over a larger volume, leading to lower effective stress concentrations. As a result, when comparing the location of maximum stress concentration before consideration of the micro-support effect against the actual crack location observed during fatigue testing, a shift in the maximum stress location may occur [50]. Various weighting parameters have been proposed for welded steel, depending mainly on the chosen stress criterion and the stress ratio. Chapter 2.1 has already shown that the microstructural support length ρ^* depends on the material and its microstructural condition and that there is a similarity between the material characteristic lengths determined according to the IGM and the TCD [29,51]:

$$a = c^2 = \left(\zeta \frac{\rho^*}{2}\right)^2 \tag{13}$$

Where ζ considers the stress criterion and can be set to $\zeta = 0.5$ [49]. Accordingly, the generally valid value for welded steel $\rho^* = 0.4$ mm, which is derived in [29] and confirmed in [52], can be used as a first approach. This results in a weighting parameter $a = 0.01$ mm^2. With more test results, it would be possible to determine the weighting factor using the scattering minimization technique, shown in [52,53].

Fig. 10 illustrates the calculated effective notch factors K_f in dependence of the weighting parameter a for two different locations. The location of the initially maximum notch factor based on elastic calculations (black curve), i.e., without consideration of the micro-support, and the actual location of the crack initiation from the DIC measurement of the fatigue test is shown in red. It is clear that the notch factor $K_{f,initial,max}$ is greater than $K_{f,crack}$ in the range of small values for the weighting parameter a. With a larger weighting parameter, the stress is averaged over a larger volume and this leads to a change in the location of the maximum notch factor after the so called "shifting point". This behavior is shown using node B2 as an example. It is evident that the value of parameter a must be greater than 0.002 mm^2, as the location of the crack initiation represents the point of maximum stress.

4.2.2. Comparison of DIC and effective notch factors

When examining specimens B1 and B2, it became apparent that considering the micro-support provides the location of crack initiation from the test as the critical site of notch stress. This correlation can be extended from general welded components to welded tubular joints within the scope of this research [16,17].

Fig. 11 shows the results of the DIC measurements for the welded joint B2. It is clear that a crack starts in the area of the weld toe at the maximum stressed point and continues to propagate over the cycles. In addition, the results of the effective notch factors K_f are shown, which demonstrate good agreement between the hot spot and the crack location from the DIC results. The same procedure was applied to specimen B1 also showing a good match between the locations, as seen in Fig. 12. A match between both examined locations is present, when the notch factors ratio at crack location and the hot-spot is higher than 0.95. This allows for accounting for potential inaccuracies throughout the entire modelling process and is based on the procedure in [17].

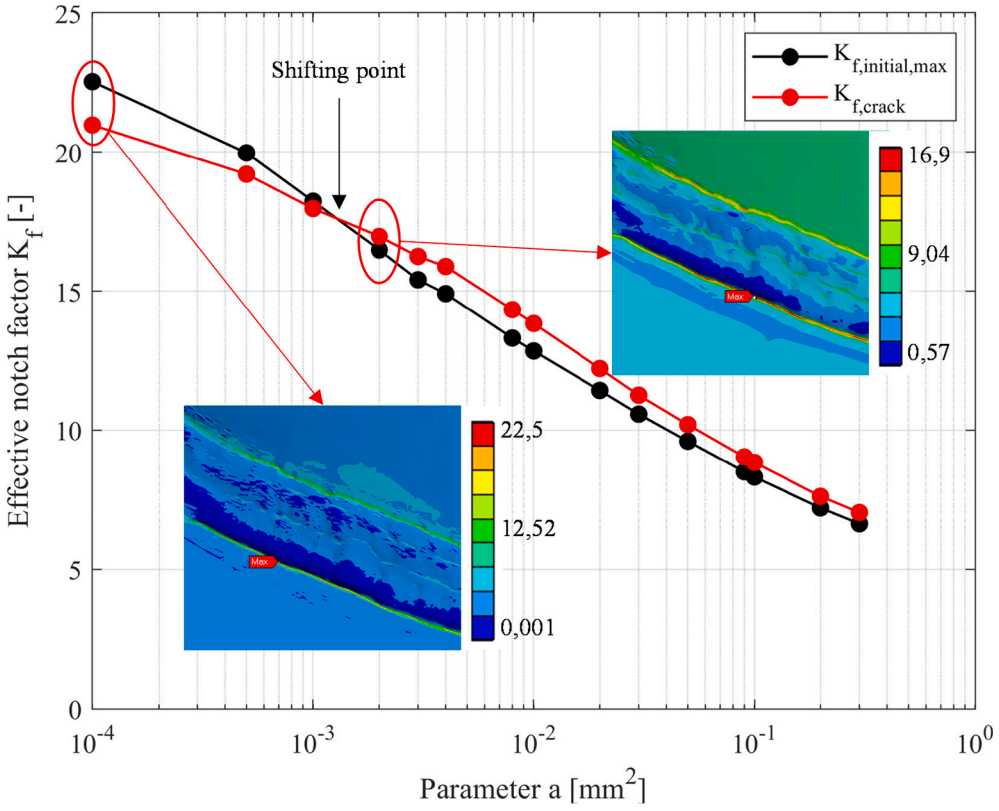

Fig. 10. Effective notch factor K_f in dependence of the weighting factor a for joint B2.

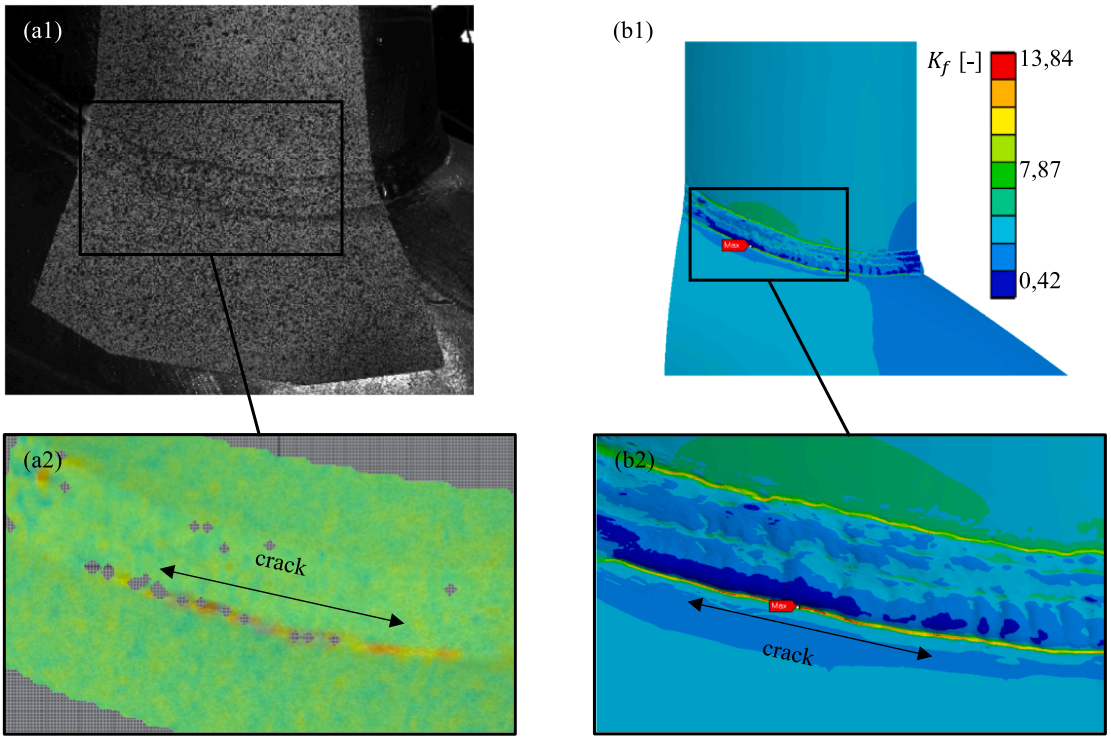

Fig. 11. Comparison of the crack location from DIC results (a1-a2) with location of the numerically determined effective notch factor (b1-b2) for tubular joint B2.

With this background, an overall notch factor ratio of > 0.95 was achieved for both welded tubular joints, so that this procedure can be used in future to determine the crack location even before the fatigue tests are carried out. The agreement between crack locations and hot spots identified by the effective notch factors is 100% for the tubular joints considered.

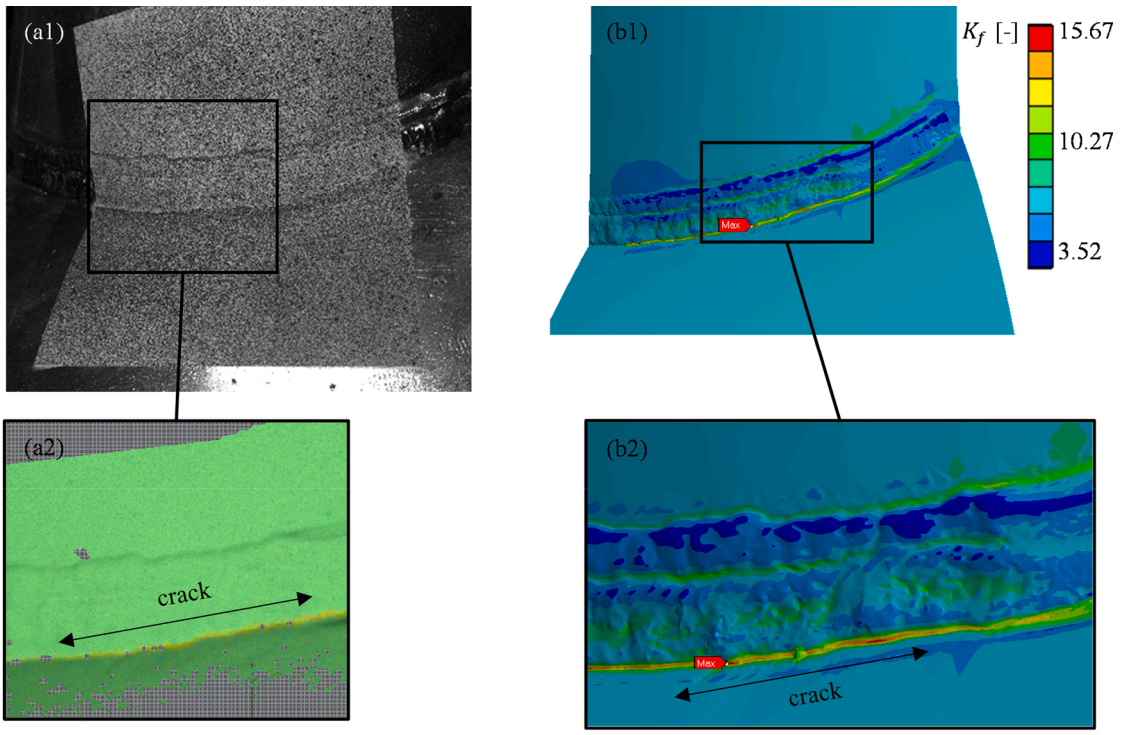

Fig. 12. Comparison of the crack location from DIC results (a1-a2) with location of the numerically determined effective notch factor (b1-b2) for tubular joint B1.

5. Fatigue lifetime assessment and discussions

Based on the explanations and results in Chapter 4.2, the weighting parameter a can be set to 0.01 mm^2 for the fatigue assessment. This value is based on assumptions from the literature for welded steel and it was shown that the crack locations could be predicted in the numerical calculation for both nodes B1 and B2. Furthermore, this weighting parameter is used to calculate the maximum effective notch factor for the entire node. This effective notch factor can then be incorporated into the 4R method process, alongside the upper and lower load limits from the fatigue test, the node's dimensions, and the residual stress values. Residual stresses for one of the nodes examined in this study have already been determined and reported in Schubnell et al. [35]. The values for both nodes are presented in Table 4.

The material parameters required for the calculations are provided from the manufacturer, including a minimum tensile strength $R_{m,min}$ = 460 MPa, a minimum yield strength $R_{p0.2,min}$ = 355 MPa, and a modulus of elasticity of 220 GPa. Using these parameters, the 4R method results in a mean stress-corrected value of the effective notch factor, which is subsequently utilized to recalculate the achievable number of load cycles until the onset of a technical crack.

According to the 4R method, values for a locally corrected R-ratio are determined, allowing the calculation of a corrected effective notch factor, as described in eq. (7). The number of load cycles until the technical crack formation is then recalculated using a 4R master curve, previously determined in [19]. The parameters from the Master Curve are integrated into the equation

$$N_f = \frac{C_f}{\Delta\sigma_{f,ref}^m} \tag{14}$$

Table 4
Input parameters for the 4R method.

	r_{brace} [mm]	t_{brace} [mm]	$K_{f,IGM}$ [-]	F_o [kN]	F_u [kN]	σ_{rs} [MPa]
B1	203	12	15.67	900	90	250
B2	203	12	13.84	870	70	250

which can be used to calculate the expected number of load cycles until the onset of a technical crack in the tubular joint. In these calculations, C_f denotes the fatigue capacity for the 4R method, $\Delta\sigma_{f,ref}$ represents the effective notch stress range after considering IGM, and m is the slope of the 4R master curve. Additionally, a calculation is performed using the same principles with the notch stress concept based on the FAT225 S-N curve recommended by the IIW. The results from both approaches are compared in Fig. 13 both with each other and also with standard assessment methods shown in [12], including the SSA and the ENS approach. Black triangles indicate the results based on the NSA, while black squares represent the results obtained using the 4R method, considering the 4R master curve described in [19]. The effective stresses for both methods were calculated using the IGM. The white circles denote the SSA results, and diamonds indicate the ENS results, with an

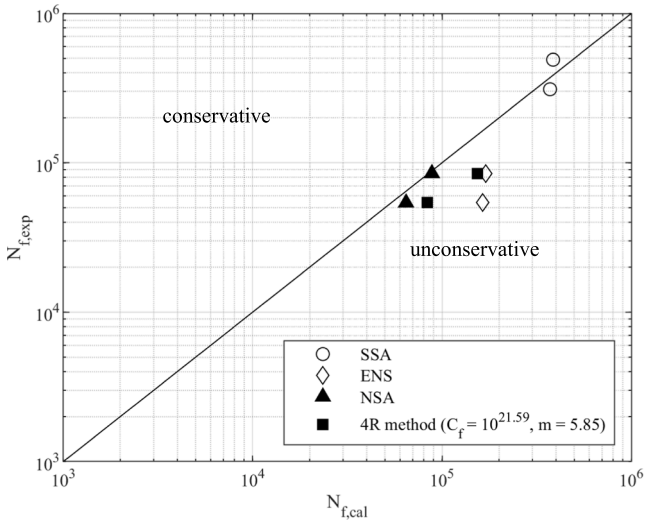

Fig. 13. Fatigue test results in comparison with predicted fatigue lives until crack initiation, effective notch stresses calculated with IGM and a = 0.01.

artificial rounding of the weld notches.

Fig. 13 shows the numerically predicted fatigue life in comparison to the fatigue test results. It reveals that there is a good compliance for all methods between the calculated number of cycles $N_{f,cal}$ and the ones from the experiment $N_{f,exp}$. The 4R method, the NSA and the ENS approach estimate the number of load cycles until a welded tubular joint develops a technical crack. The SSA in comparison estimates the number of load cycles until through-thickness crack is reached. The slightly overestimation by the NSA using IGA highlights the methods' suitability for predicting service life. Notably, the 4R method lies on the unconservative side and demonstrates less accuracy. It should be noted that the approach with $a = 0.01$ mm^2 for the IGM applies to steel in general and was derived using different steel samples excluding welded tubular joints. The ENS approach with fictitious notch rounding overestimates the fatigue life until crack initiation for both welded tubular joints and appears to be applicable in the present form for the welded tubular joints. The weld geometry approximated in the CAD model cannot depict reality and the notch stresses calculated are too small. As a result, the calculated load cycle numbers $N_{f,cal}$ are significantly greater than those in the experiment $N_{f,exp}$. The SSA delivers results that are in both the conservative and unconservative range. At this stage, it is not yet possible to make a precise statement on the applicability of this method; further fatigue tests are required.

This study marks a pioneering application of the presented methods to welded tubular joints, offering promising initial insights despite involving only two specimens. Both the 4R method and the notch stress concept, in conjunction with the determination of effective notch factors by IGM, offer the possibility of predicting the number of load cycles in fatigue tests up to technical crack. Overall, a framework could be created to incorporate various parameters into the fatigue assessment for welded tubular joints and a technical crack of 40 mm proved to be a suitable assumption based on the background of the notch stress concept, which needs further evaluation. A first approach would be to analyze the crack growth of the welded tubular joints during the fatigue test in order to include the actual crack shape in the technical crack criterion. From recent publications, such as Thibaux et al. [54], it is clear that fatigue cracks in welded tubular joints will primarily grow on the surface and might become very long prior to penetrating through the thickness. In the next application, the framework developed could therefore be supplemented with fracture mechanics methods in order to map the entire service life of a welded tubular joint. However, there are some further comments to be made on the fatigue assessment and application of the methods presented in this respect: Section 3.4 revealed that the fatigue test results for the manually welded tubular joints fall slightly below the applicable T S-N curve specified in DNV-RP-C203 [4]. For the evaluation, a 50% probability level was applied, as determining the 97.7% survival probability using the student's t-distribution would introduce significant scatter due to the limited number of specimens. It is anticipated that further testing will give more insights into the fatigue strength of these tubular joints. It is also important to note that the joints were fabricated following DIN EN 1090–2 [36] standards, rather than offshore specifications, with a welding configuration comprising two-thirds single bevel butt weld and one-third fillet weld, and were welded on only one side. Additionally, joint B1 was preloaded during preliminary tests and joint B3 failed along a post-treated weld seam, which affects the comparability of the results. The residual stress measurements were only carried out on one tubular joint and were used in this framework for fatigue assessment for both joints. The location analyzed was identified as a hot-spot without considering the real weld seam geometry. Measurement data specific to each specimen – such as hardness measurements in fatigue-critical areas or residual stress assessments at crack initiation points – could refine analysis precision further. Within this aspect the material behavior in the notch may theoretically also be included via correlation of the HV hardness and the tensile strength R_m. The influence of weld seam geometry was tailored to individual specimens, leveraging available scans to determine effective notch factors precisely. Using the 4R method, it is also possible to consider different states of residual stresses in order to include post-treated weld seams in the evaluation in the future.

It is additionally important to recognize that the 4R master curve utilized for estimating load cycles was originally derived from butt weld specimens via the 4R method as outlined in [19]. While the findings affirm its applicability to welded tubular X-joints, the limited sample size suggests a need for additional results to statistically validate whether such application holds without modification. Furthermore, the FAT225 S-N curve was used for the evaluation of the calculated numbers of load cycles $N_{f,cal}$ and was assumed to be suitable. The FAT225 S-N curve is applied here as it is the standard curve to use in combination with the notch stress approach with fictitious notch rounding according to IIW recommendation [12]. In this study, the fictitious notch rounding is not used directly, but the implicit gradient approach with the same parameters. In addition to the FAT225, there are other S-N curves, such as the FAT160, which was derived according to Baumgartner [52] for the Point and Line method of the TCD. Therefore, the aspect of a suitable S-N curve to be applied in the presented framework has to be examined in following analyses. This will be done later in the project as the experimental program progresses and more results become available. In addition, the assumption of $a = 0.01$ mm^2 cannot be unambiguously applied to the case "as welded tubular X-joints", even if a high agreement between the crack location and the hot-spots of the effective notch factor could be achieved. The analyses from chapter 4.2 have shown that the locations also agree for larger and smaller values of the weighting factor.

In this context, employing the scattering minimization technique could enhance parameter determination based on several different welded tubular X-joints, fortifying the proposed frameworks utility in these novel applications.

6. Conclusion

In this study, welded tubular X-joints underwent an innovative analysis process, blending advanced 3D digital scanning, high-cycle fatigue testing, and advanced numerical evaluation to yield crucial insights. The reason behind the application of the mentioned methods was the creation of a framework to be able to consider geometrically modified weld seams, so-called design-welds, in the fatigue analysis. Elastic notch factors were calculated and refined to determine effective notch factors using the implicit gradient model framework. These refined factors were then integrated into the 4R method and the notch stress concept to recalculate the test specimen's service life up to the technical crack. The DIC data from fatigue tests was analyzed to determine the number of load cycles until the formation of a 40 mm technical crack. This comprehensive approach allowed for a robust assessment and provided several key findings:

- The evaluation of the fatigue tests showed a slight undercutting of the S-N curve specified in the DNV-RP-C203 standard and a mean fatigue strength of $\Delta\sigma_C = 93.5$ N/mm^2 was determined.
- It was assumed that the results from the notch stress concept could be applied to welded tubular joints. This assumption was based on the idea that a fracture of a small-scale fatigue test specimen is equivalent to crack initiation in a large-scale structure with 40 mm. With this assumption, the crack initiation phase accounts for about 17% of the component's total service life in both tubular joints.
- The locations of the maximum elastic notch factors calculated from the digital scans of the nodes, including the weld seam geometry, do not initially match the crack initiation locations. However, with consideration of the fatigue effective stresses, by applying the implicit gradient model presented in this study, the location of the maximum notch factor shifted to the crack initiation point identified during testing.

- Calculating the number of load cycles until the technical crack in the tested welded tubular X-joints showed that both the 4R method and the notch stress concept are suitable for predicting service life until crack initiation of a technical crack. Using the 4R method, it is also possible to consider different states of residual stresses in order to include post-treated weld seams in the evaluation.
- The findings demonstrate a scalable framework that enhances fatigue life predictions, making it highly applicable for industry adoption across various welded structures, including bridges and automotive components. High-precision 3D scanning technologies, including automated ones, are now widely available. By addressing real-world imperfections through advanced modelling, the framework offers versatile solutions for increasing structural reliability through more accurate calculations of service life of critical infrastructure beyond jacket structures.

The results of this study represent an important initial step in applying the already established methods to large structures like welded tubular X-joints and potential design-welds. The developed methodology can be used to predict the high-cycle fatigue lifetime of welded joints, which can be used for new or existing structures with welded details.

Declaration of generative AI in scientific writing

During the preparation of this work, the authors used ChatGPT to improve readability and language. After using this tool, the authors reviewed and edited the contents as needed and take full responsibility for the contents of the published article.

CRediT authorship contribution statement

Tim Brömer: Writing – original draft, Visualization, Validation, Project administration, Methodology, Investigation, Formal analysis, Conceptualization. **Viktor Widerspan:** Writing – review & editing, Investigation. **Sulaiman Shojai:** Writing – review & editing, Conceptualization. **Elyas Ghafoori:** Writing – review & editing, Supervision, Project administration.

Declaration of competing interest

The authors declare that they have no known competing financial interests or personal relationships that could have appeared to influence the work reported in this paper.

Acknowledgements

This study is part of a German national joint research project “SmartWeld – Innovative design and manufacturing concept to increase light-weight potentials in steel constructions “. The research is funded by the German Federal Ministry for Economics and Climate Action (Project No. 03LB2022D). Additionally, this work was also supported by funding from Ministry for Science and Culture of Lower Saxony (Niedersächsisches Ministerium für Wissenschaft und Kultur, MWK), Germany, with the grant number ZN3725.

Data availability

Data will be made available on request.

References

[1] C. Ma, J. Ban and G. Zi, “Comparative study on the dynamic responses of monopiles and jacket-supported offshore wind turbines considering the pile-soil interaction in transitional waters,” *Ocean Engineering,* no. 292, 2024.
[2] Seidel M. Substructures for offshore wind turbines - Current trends and developments. Festschrift Peter Schaumann; 2014.
[3] IEA, “Net Zero by 2050,” IEA, 2021. [Online]. Available: https://www.iea.org/reports/net-zero-by-2050. [Accessed 15 October 2024].
[4] DNV-RP-C203, “Fatigue design of offshore steel structures,” DNV, Oslo, 2024.
[5] OTH 92 390, “Background to New Fatigue Guidance for Steel Joints and Connections in Offshore Structures,” Health and Safety Executive (HSE), 1999.
[6] A. van Wingerde, D. van Delft, J. Wardenier and J. Packer, “Scale Effects on the Fatigue Behaviour of Tubular Structures,” in *IIW International Conference on Performance of Dynamically Loaded Welded Structures*, San Francisco, USA, 1997.
[7] G. Zilli, S. Karamanos, P. Thibaux, M. Vossbeck, C. Ruiz, F. Gelagoti, R. Kourkoulis, S. Mavrakos and D. Manolas, “JABACO - Development of Modular Steel Jacket for Offshore Windfarms. Final Report”.
[8] Schürmann K. Fatigue behavior of automatically welded tubular joints for offshore wind energy substructures. Hannover: Gottfried Wilhelm Leibniz Universität; 2021.
[9] Bäumel A, Seeger T. Materials Data for Cyclic Loading: Supplement 1. Amsterdam: Elsevier; 1990.
[10] Fiedler M, Varfolomeev I, Wächter M. Richtlinie Nichtlinear: Vorhaben Nr. 301. Rechnerischer Bauteilfestigkeitsnachweis unter expliziter Erfassung nichtlinearen Werkstoff-Verformungsverhalten. Frankfurt, Main: FKM; 2016.
[11] Z. Lopez and A. Fatemi, “A method of predicting cyclic stress-strain curve from tensile properties for steels,” *Materials Science & Engineering A,* 14 July 2012.
[12] Hobbacher A. Recommendations for Fatigue Design of Welded Joints and Components. Cham: Springer; 2016.
[13] DIN EN 1993-1-9, “Eurocode 3: Design of steel structures - Part 1-9: Fatigue,” Deutsches Institut für Normung e.V., Berlin, 2010.
[14] Radaj D, Sonsino C. Ermüdungsfestigkeit von Schweißverbindungen nach lokalen Konzepten. Düsselsdorf: DVS Verlag; 2000.
[15] Knobloch M, Röscher S, Steinhoff S, Seidel M, Rauch M. “Erweiterte Konzepte der Betriebsfestigkeit,” in *Stahlbau Kalender*. Berlin: Ernst & Sohn; 2024.
[16] Shojai S, Brömer T, Ghafoori E, Woitzik C, Braun M, Köhler M, et al. Assessment of corrosion fatigue in welded joints using 3D surface scans, digital image correlation, hardness measurements, and residual stress analysis. *Int J Fatigue* 2023.
[17] Shojai S, Brömer T, Ghafoori E, Schaumann P. Application of local fatigue approaches on corroded welded joints with consideration of weld geometry and residual stresses. *Theor Appl Fract Mech* October 2023.
[18] C. Dänekas, J. Schubnell, J. Krautheimer, M. Jung, E. Ghafoori und P. Schaumann, „Algorithms for determination of weld toe radius and weld toe angle in welded joints,“ *Journal of Constructional Steel Research,* January 2025.
[19] Nykänen T, Björk T. A new proposal for assessment of the fatigue strength of steel buttwelded joints improved by peening (HFMI) under constant amplitude tensile loading. *Fatigue Fract Eng Mater Struct* 2016.
[20] Larsen ML, Arora V, Lützen M, Pedersen RR, Putnam E. “38th International Conference on Ocean, Offshore and Arctic Engineering,” in *Use of 3D Scan of Weld Joint in Finite Element Analysis and Stochastic Analysis of Hot-Spot Stresses in Tubular Joint for Fatigue Life Estimation*. Scotland, UK: Glasgow; 2019.
[21] Plets J, Hectors K, De Waele W. “20th EAWE PhD Seminar,” in *Remaining fatigue lifetime of welded tubular joints of offshore structures using detailed stress analysis based on 3D scans*. Visby 2024.
[22] R. Peerlings, W. Brekelmans, R. de Borst and M. Geers, “Gradient-enhanced damage modelling of high-cycle fatigue,” *International Journal For Numerical Methods In Engineering,* pp. 1547-1569, 29 February 2000.
[23] Lang R. Ein Beitrag zur Bestimmung der Anrisslebensdauer geschweißter Bauteile. Faculty of Technical Sciences: Leopold-Franzens-University Innsbruck, Innsbruck; 2015.
[24] Neuber H. Kerbspannungslehre: Grundlagen für genaue Festigkeitsberechnung mit Berücksichtigung von Konstruktionsform und Werkstoff. Heidelberg: Springer-Verlag, Berlin; 1958.
[25] Björk T, Ahola A, Skriko T. “4R METHOD FOR CONSIDERATION OF THE FATIGUE PERFORMANCE OF WELDED JOINTS – BACKGROUND AND APPLICATIONS,” in *Ninth International Conference on Advances in Steel Structures (ICASS'2018)*. Hong Kong: China; 2018.
[26] Radaj D, Vormwald M. Ermüdungsfestigkeit: Grundlagen für Ingenieure. Heidelberg: Springer-Verlag, Berlin; 2007.
[27] Neuber H. Über die Berücksichtigung der Spanungskonzentration bei Festigkeitsberechnungen. *Konstruktion* 1968.
[28] D. Taylor, “The theory of critical distances,” *Engineering Fracture Mechanics,* pp. 1696-1705, 2008.
[29] Radaj D. “Generalised Neuber Concept of Ficticious Notch Rounding,” in *Advanced Methods of Fatigue Assessment*. Heidelberg: Springer, Berlin; 2013. p. 1–100.
[30] Radaj D. Design and Analysis of Fatigue Resistant Welded Structures. Woodhead Publishing; 1990.
[31] Bažant Z. Imbricate Continuum and its Variational Derivation. *J Eng Mech* 1984: 1693–712.
[32] Zhang G. Method of effective stress for fatigue: Part I - A general theory. *Int J Fatigue* 2012:17–23.
[33] Smith K, Watson P, Topper T. A stress-strain function for the fatigue of metals (stress-strain function for metal fatigue including mean stress effect). *J Mater* 1970.
[34] Ramberg W, Osgood W. Description of stress-strain curves by three parameters. Washington, D.C.: National Advisory Committee for aeronautics; 1943.
[35] Schubnell J, Carl E, Widerspan V, Collmann M. Determination of Loading and Residual Stresses on Offshore Jacket Structures by X-ray Diffraction. *Journal of Marine Science and Engineering* 2023.
[36] DIN EN 1090-2, “Execution of steel structures and aluminium structures - Part 2: Technical requirements for steel structures,” Deutsches Institut für Normung e.V., Berlin, 2024.
[37] Olivier R, Köttgen V, Seeger T. “Schwingfestigkeitsnachweise für Schweißverbindungen auf der Grundlage örtlicher Beanspruchungen –

Schweißverbindungen I," *FKM-Forschungsheft 143. Forschungskuratorium Maschinenbau* 1989.
[38] Olivier R, Köttgen V, Seeger T. "Untersuchungen zur Einbindung eines neuartigen Zeit- und Dauerfestigkeitsnachweises von Schweißverbindungen aus Stahl in Regelwerke – Schweißverbindungen II," *Schwingfestigkeitsnachweise FKM-Forschungsheft 180. Forschungskuratorium Maschinenbau* 1994.
[39] Sonsino C, Fricke W, de Bruyne F, Hoppe A, Ahmadi A, Zhang G. Notch stress concepts for the fatigue assessment of welded joints - Background and applications. *Int J Fatigue* 2012:2–16.
[40] Braun M. Assessment of fatigue strength of welded joints at sub-zero temperatures based on the micro-structural support effect hypothesis. Hamburg: Technische Universität Hamburg; 2021.
[41] Hutt T, Cawley P. Feasibility of digital image correlation for detection of cracks at fastener holes. *NDT&E International* November 2009:141–9.
[42] N. Friedrich and S. Ehlers, "Crack monitoring in resonance fatigue testing of welded specimens using digital image correlation," *JoVE (Journal of Visualized Experiments) 151,* 2019.
[43] Kovářík O, Haušild P, Medřický J. Fatigue Crack Growth in Bodies with Thermally Sprayed Coating. *J Therm Spray Technol* January 2016;25:311–20.
[44] ECCS Technical Committee 6, "Background Documentation 9.01a - 25 Background information on fatigue design rules - Statistical evaluation," 2018.
[45] Peerlings R. Enhanced damage modelling for fracture and fatigue. Technische Universiteit Eindhoven 1999.
[46] Lang R, Ladinek M, Lener G. Über die Anpassung eines fortschrittlichen Stützwirkungsansatzes für das Kerbspannungskonzept. *Stahlbau* May 2017;30.
[47] Lener G, Lang R, Ladinek M, Timmers R. A numerical method for determining the fatigue strength of welded joints with a significant improvement in accuracy. *Procedia Eng* 2018.
[48] Askes H, Susmel L. Understanding cracked materials: Is Linear Elastic Fracture Mechanics obsolete? *Fatigue Fract Eng Mater Struct* 2014.
[49] Susmel L, Askes H, Bennett T, Taylor D. Theory of Critical Distances versus Gradient Mechanics in modelling the transition from short to long crack regime at the fatigue limit. *Fatigue Fract Eng Mater Struct* December 2012;31.
[50] S. Shojai, P. Schaumann and E. Ghafoori, "Micro-support effect consideration in fatigue analysis of corroded steel based on real surface geometry," *Journal of Constructional Steel Research,* January 2024.
[51] Askes A, Livieri P, Susmel L, Taylor D, Tovo R. Intrinsic material length, Theory of Critical Distances and Gradient Mechanics: analogies and differences in processing linear-eöastic crack tip stress fields. *Fatigue Fract Eng Mater Struct* Januar 2013.: 39–55.
[52] Baumgartner J, Schmidt H, Ince E, Melz T, Dilger K. "Fatigue assessment of welded joints using stress averaging and critical distance approaches," *Weld. WORLD* 2015.
[53] Tovo R, Livieri P. An implicit gradient application to fatigue of sharp notches and weldments. *Eng Fract Mech* 2007:515–26.
[54] P. Thibaux, M. Thiele, J. Van Wittenberghe and M. Baessler, "Comparison of resonance and hydraulic testing on large scale fatigue tests of welded tubular joints for offshore wind turbine foundations," *International ournal of Fatigue,* April 2025.